

Charge Coupled Devices for detection of coherent neutrino-nucleus scattering

Guillermo Fernandez Moroni^{1,2,3}, Juan Estrada³, Gustavo Cancelo³,

Eduardo Paolini^{2,4}, Javier Tiffenberg³, Jorge Molina⁵

¹*Comisión de Investigaciones Científicas y Técnicas (CONICET), Argentina*

²*Universidad Nacional del Sur, Av. Alem 1253, (8000) Bahía Blanca, Argentina*

³*Fermi National Accelerator Laboratory, Batavia IL, United States.*

⁴*Comisión de Investigaciones Científicas Prov. Buenos Aires (CIC), Buenos Aires, Argentina and*

⁵*Universidad Nacional de Asunción, Asunción, Paraguay*

This article details the potential for using Charge Coupled Devices (CCD) to detect low-energy neutrinos through their coherent scattering with nuclei. The detection of neutrinos through this standard model process has not been accessible because of the small energy deposited in such interactions with the detector nuclei. Typical particle detectors have thresholds of a few keV, and most of the energy deposition expected from coherent scattering is well below this level. The devices we discuss can be operated at a threshold of approximately 30 eV, making them ideal for observing this signal. For example, the number of coherent scattering events expected on a 52 gram CCD array located next to a power nuclear reactor is estimated to be near to 626 events/year. The results of our study show that detection at a confidence level of 99% can be reached within three months for this kind of detector array.

I. INTRODUCTION

Since the discovery of neutral-current neutrino interactions in 1973 by Hasert *et al.* [1], the importance of the coherent enhancement in elastic neutrino scattering has been pointed out [2], along with its implication for studies of star collapse. Unfortunately, it is difficult to detect because of its very small cross section ($< 10^{-39}$ cm²) [3] and the small energy deposition, typically less than < 10 keV for any material. Detector technology has not met yet the extreme requirements on detector mass or on the energy threshold. Nevertheless, in recent times, interest from low energy neutrino physics has been increasing, mainly for verifying predictions of the standard model (SM), and exploring the possibilities of new physics beyond the SM at very small energy scales [4]. In astrophysics, for example, the understanding of MeV-neutrino physics has great relevance for energy transport in supernovas and it is related to the ongoing effort to develop new supernova detectors. These kind of detectors can also be used to monitor nuclear reactors through their emitted neutrinos [5, 6].

Although initially devised as memory devices [7, 8], CCD have found a niche as imaging detectors due to their ability to obtain high resolution digital images of objects placed in their line of sight. In particular, scientific CCDs have been used extensively in ground and space-based astronomy and X-ray imaging [9]. These devices have high detection efficiency, low noise, good spatial resolution, and low dark current. Furthermore, thick CCDs with increased detection mass enable their use as particle detectors [17]. Using this technology, the DAMIC search for cold dark matter has been deployed at Snolab [10].

Several nuclear-reactor neutrino experiments were based mostly on inverse beta decay [11–13], usually using large volumes of target materials to counter their relatively high threshold energy of several keV. Recently, with the decreasing threshold of solid-state detectors

there has been a growing interest in using them for neutrino detection [14, 15]. In this paper, we discuss the potential for using CCD technology for neutrinos scattering. We analyze the potential detection of neutrinos at a detector threshold of 28 eV of ionizing energy (five times larger than the RMS noise of 5.5 eV). The low-energy threshold of a CCD provides an opportunity to detect the main mechanism of neutrino-nucleus coherent scattering, which has never been observed. The proposed detector uses a mass of approximately 100 g of Si, which allows the construction of a small-sized nuclear-reactor neutrino detector. Our focus is on neutrinos with energies of < 12 MeV produced at a nuclear reactor.

II. HIGH RESISTIVITY SCIENTIFIC CCD

Figure 1 shows a scientific CCD developed by Lawrence Berkeley National Laboratory and characterized extensively at Fermilab for the DECam project [17, 18]. Figure 1(a) shows the cross section of the layout of the three gates that compose one pixel. Figure 1(b) depicts the potential well generated under the gates in normal operation. Several million pixels CCD are fabricated on high resistivity silicon to maximize the depleted silicon volume and therefore increase the near-IR photon response. CCDs with thickness of approximately 650 μ m are available, and provide up to 5.2 grams of detector mass. The CCD is fully depleted with the use of a substrate voltage. The array is divided into square pixels of 15 μ m by 15 μ m, which provides sufficient spatial resolution for efficient rejection of some of the background particles. An example of this characteristic is shown in Fig. 2, which presents a compendium of background events from measurements at sea level.

Each particle produces a distinctive two-dimensional pattern in the CCD array. A muon is characterized by a straight-line track crossing the entire silicon volume.

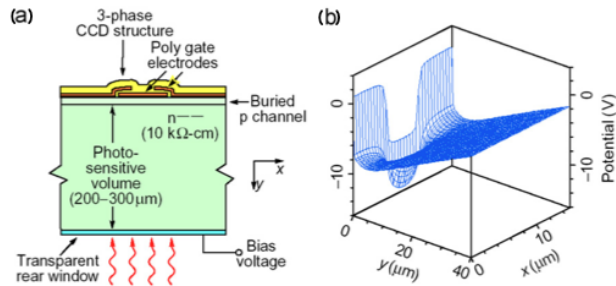


FIG. 1. Cross section of a $250 \mu\text{m}$ thick CCD developed at Lawrence Berkeley National Laboratory, (a) layout of the three gates that form one pixel, (b) electrostatic potential (V) generated through the three gated phases is shown as function of depth (y axis) and one of the lateral directions (x axis). Figure from reference [16].

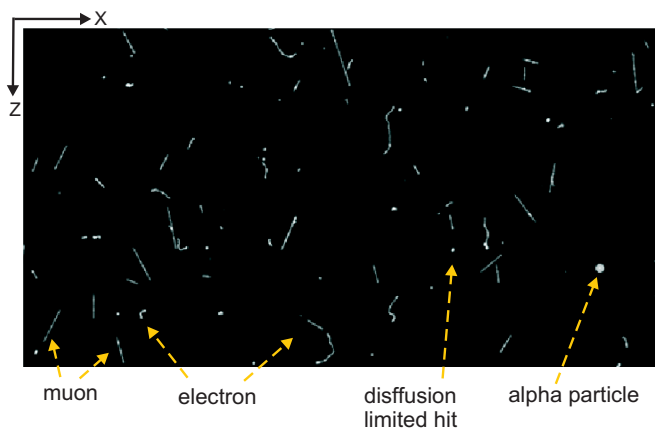


FIG. 2. Compendium of images from recent measurement of background at sea level in a CCD (See text for an interpretation of the events).

The small curved tracks are typical of energetic electrons produced by electromagnetic radiation. Alpha particles appear as big circular bright dots, due to the plasma effect they produce in the silicon [19]. Finally, point events (energy deposited in a single pixel volume) are produced by the ionized charge that flows to neighbor pixels by diffusion. The coherent neutrino-nucleus scattering is expected to produce these kind of point events, as described in Section V B.

Besides the relatively large mass and high spatial resolution, these devices have a very small energy threshold, which is another attractive feature for neutrino detection. This characteristic is due to the small CCD read-out noise, good charge transfer efficiency, and negligible dark-current contribution in a cooled system. The read-out noise is added to each pixel by the output amplifier during the charge packet readout. It has a Gaussian distribution with a standard deviation (σ_{RMS}) that depends on the readout time of the pixel, as shown in Fig. 3 (see [20, 21] for a detailed analysis). Because of the interaction between $1/f$ and white noise, an optimum read-out

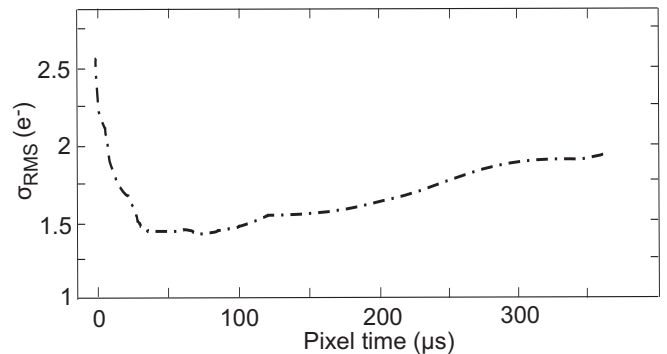


FIG. 3. RMS pixel error (σ_{RMS}) caused by the output amplifier, as a function of pixel read-out time.

noise with $\sigma_{RMS} = 1.5 e^-$ (equivalent to 5.5 eV of ionization energy) can be achieved using a pixel read-out time of $30 \mu\text{s}$. In what follows, it is assumed that this noise level is achieved during normal operation of the detector.

Current fabrication techniques and materials have yielded CCD detectors with dark-current generation below $2 e^-/\text{day}/\text{pixel}$ when cooled at 123 K, and transfer inefficiencies below 15 ppm that have negligible effect on the detection of low energy particles.

III. NEUTRINO INTERACTION WITH MATTER

A nuclear power reactor is a high flux source of electron antineutrinos ($\bar{\nu}_e$) with energies up to 12 MeV, approximately. At such energies, the largest probability for interaction with Si atoms is given by the coherent neutrino-nucleus interaction. In this process, a neutrino of any flavor scatters off a Si nucleus transferring some energy in the form of a nuclear recoil. The SM cross section σ for this process is [2, 22]

$$\frac{d\sigma}{dE_{\bar{\nu}_e} dE_{\text{rec}}}(E_{\bar{\nu}_e}, E_{\text{rec}}) = \frac{G_F^2}{8\pi} [Z(4\sin^2\theta_W - 1) + N]^2 \times M \left(2 - \frac{E_{\text{rec}}M}{E_{\bar{\nu}_e}^2}\right) |f(q)|^2 \quad (1)$$

where M , N and Z are, respectively, the mass, neutron number and atomic number of the nucleus, $E_{\bar{\nu}_e}$ and E_{rec} are the incident neutrino and the nuclear recoil energy, G_F is the Fermi coupling constant, θ_W is the weak mixing angle, and $f(q)$ is the nuclear form factor at momentum transfer q . According to [23], $|f(q)| \approx 1$, within an uncertainty of a few percent. This is applicable for $E_{\bar{\nu}_e} < 50$ MeV, where the momentum transfer (q^2) is small enough such that $q^2 R^2 < 1$, where R is the radius of the nucleus [4]. At small momentum transfers, the individual nucleon amplitudes are in phase and add coherently, so that the cross section increases by a factor of approximately N^2 .

Although the cross section is enhanced by such coherence, elastic neutrino-nucleus scattering is difficult to

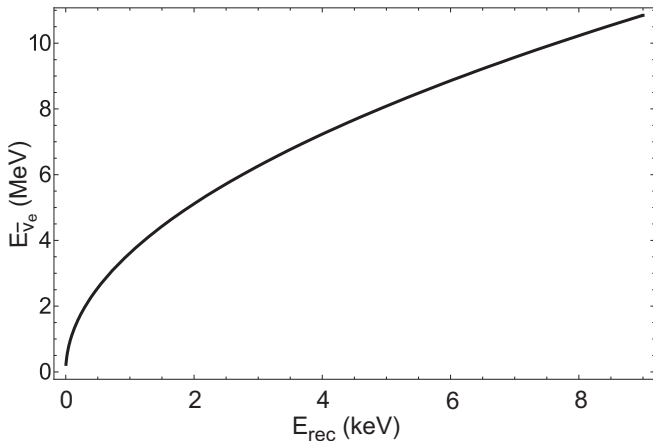


FIG. 4. Neutrino energy as a function of maximum transferred energy to the Si nucleus.

observe because of the very small nuclear recoil energies. Figure 4 depicts this relationship for silicon atoms, where the maximum event energy is $\max(E_{\text{rec}}) = 2E_{\bar{\nu}_e}^2/M$ (approximately 10 keV). Therefore, this kind of measurement requires very sensitive detectors and a good characterization of the background.

The total cross section $\sigma_T(E_{\bar{\nu}_e})$ for a mono-energetic neutrino source of energy $E_{\bar{\nu}_e}$ is given by

$$\sigma_T(E_{\bar{\nu}_e}) = \frac{G_F^2}{4\pi} [Z(4\sin^2\theta_W - 1) + N]^2 E_{\bar{\nu}_e}^2$$

that can be approximated by

$$\sigma_T(E_{\bar{\nu}_e}) \approx 4.22 \times 10^{-45} N^2 E_{\bar{\nu}_e}^2 \quad (2)$$

when $E_{\bar{\nu}_e}$ is expressed in MeV and σ_T in cm^2 . The total cross section σ_T for ^{28}Si ($N = 14$) is shown in light-blue trace in Fig. 5 as a function of the neutrino energy $E_{\bar{\nu}_e}$, showing the small probability for interaction of low energy neutrinos with matter, and its strong dependence on incident energy. The total cross section σ_T weighted by the $\bar{\nu}_e$ energy spectrum from a reactor ($dN_{\bar{\nu}_e}/dE_{\bar{\nu}_e}$) is also depicted in Fig. 5 using a black solid line, which is related to the probability of observing a reactor $\bar{\nu}_e$ of a given energy. The most probable event arises from neutrino energies between 2 MeV and 4 MeV. If the CCD threshold level is considered, the probability of detection is reduced, as depicted by the dashed curves in Fig. 5. In this case, the total cross section is calculated using a threshold of 28 eV, approximately 5 times the minimum RMS noise level σ_{RMS} . These results, summarized in Fig. 5, suggest that the low threshold of the detectors is adequate for detecting $\bar{\nu}_e$ scattering.

IV. NEUTRINO SOURCE: NUCLEAR REACTOR

Nuclear reactors emit about 3.1×10^{16} $\bar{\nu}_e$ /s per MW of thermal power, broadly distributed over energies up to

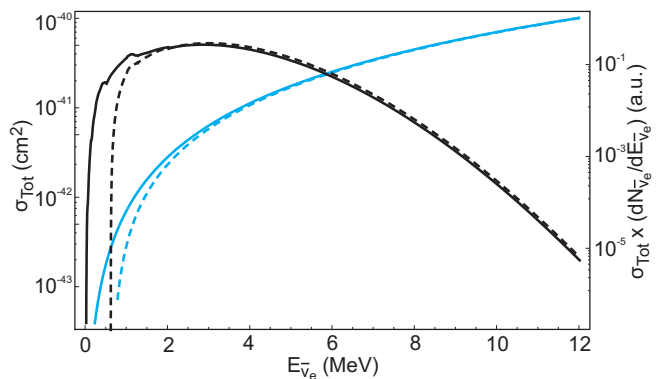


FIG. 5. Total neutrino-nucleus coherent cross section σ_T for silicon from Eq. 2 (light blue curve, left), and weighted by the reactor antineutrino spectrum (black curve, right). The dashed lines correspond to a threshold energy of 28 eV, approximately $5\sigma_{\text{RMS}}$ of the detector noise.

12 MeV, with a maximum between 0.5 MeV to 1 MeV. The antineutrinos come out isotropically from the core, so that the expected flux density at a distance L is diminished by the factor $1/(4\pi L^2)$. At steady state operation, approximately 7.3 $\bar{\nu}_e$ ($N_{\bar{\nu}_e}$) are produced per reactor fission [15]. Many processes are involved in antineutrino production, but the two major contributions are β decays of fission fragments of the four fissile isotopes ^{235}U , ^{238}U , ^{239}Pu , ^{241}Pu (≈ 6.1 $\bar{\nu}_e$ /fission), and neutron capture by ^{238}U (≈ 1.2 $\bar{\nu}_e$ /fission). The relative contribution from each source varies in different reactors, as well as in a single reactor during a burning cycle, resulting in antineutrino flux scenarios that differ by a few percent. Although such variations are clearly noticeable, they are small enough to provide an essentially model-independent analysis of any reactor neutrino experiment. In the following sections, each production mechanism is analyzed in more detail.

A. Antineutrinos from fissile isotopes

The $\bar{\nu}_e$ emitted in power reactors are predominantly produced through β -decays of the fission products, following the fission of the four dominant fissile isotopes: ^{235}U , ^{238}U , ^{239}Pu , and ^{241}Pu . Other fissile isotopes such as ^{236}U , ^{240}Pu , ^{242}Pu , etc, contribute less than 0.1% to the fissile isotope spectrum, and therefore can be neglected. Each isotope has a different $\bar{\nu}_e$ yield, $\bar{\nu}_e$ spectrum, and fission rate. Their content also changes during the fuel burning cycle, and leads to a small variation of the $\bar{\nu}_e$ flux and spectrum. This affects the total number $N_{\bar{\nu}_e}$ by a few percent, and can be ignored in a first order analysis of a CCD-based detector. The typical $\bar{\nu}_e$ yield per element fission, as well as their relative contributions per reactor fission are summarized in Table I. The $\bar{\nu}_e$ spectrum produced through the fission of each isotope is depicted in Fig. 6 in units of $\bar{\nu}_e$ /MeV for each process.

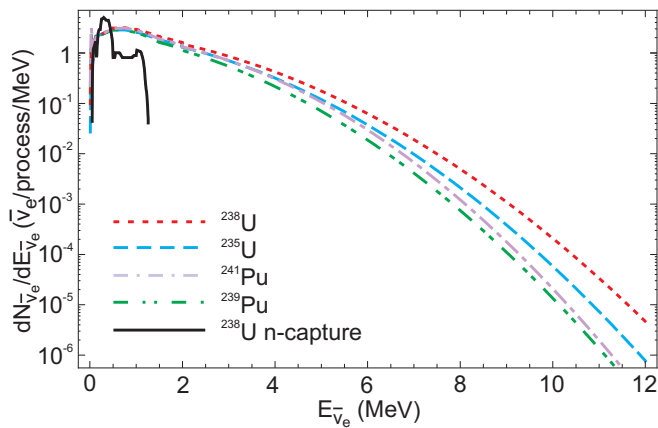


FIG. 6. Antineutrino spectrum for each process.

TABLE I. Relative fission contribution and neutrino yield per fission for the four fissile isotopes and the ^{238}U neutron capture. Typical values are given for integrated contributions.

Process	Relative rate for reactor fission	Neutrino yield ($N_{\bar{\nu}_e}/\text{process}$)	Neutrino yield ($N_{\bar{\nu}_e}/\text{fission}$)
^{235}U	0.56	6.14	3.43
^{238}U	0.08	7.08	0.56
^{239}Pu	0.30	5.58	1.67
^{241}Pu	0.06	6.42	0.38
$^{238}\text{U}(n,\gamma)$	0.60	2.00	1.20

The antineutrino spectra are taken from [24, 25]. For energies above 2 MeV, the parametrization is represented by the model

$$dN_{\bar{\nu}_e}/dE_{\bar{\nu}_e} = e^{a_0 + a_1 E_{\bar{\nu}_e} + a_2 E_{\bar{\nu}_e}^2}, \quad (3)$$

where a_0 , a_1 , a_2 are the fitted parameters, with values shown in Table II. For energies below 2 MeV, the antineutrino spectrum is given in tabulated form, and the values are listed in Table III.

B. Antineutrinos from neutron capture in ^{238}U

The ^{238}U content in power reactors nuclear fuel varies between 95 % to 97 %. The ^{238}U nuclei absorb approximately 0.6 neutrons per fission via the (n,γ) reaction: $^{238}\text{U} + n \Rightarrow ^{239}\text{U} \Rightarrow ^{239}\text{Np} \Rightarrow ^{239}\text{Pu}$. Two $\bar{\nu}_e$ are produced through β -decay of ^{239}U . This process contributes nearly 16% to the total $\bar{\nu}_e$ flux. The $\bar{\nu}_e$ yield and rate per fission at the reactor are also summarized in Table I. The energy of the antineutrinos produced by this process is below 1.3 MeV, as shown in Fig. 6 (black curve). A description of these processes can be found in [15].

Figure 7 depicts the total antineutrino spectrum per fission with (dashed line) and without (solid line) the contribution of the ^{238}U capture mechanism. This graph

TABLE II. Constants for Eq. (3) for each fissile isotope.

a_i	^{235}U	^{239}Pu	^{238}U	^{241}Pu
a_0	1.260	1.0800	1.500	1.3200
a_1	-0.160	-0.2390	-0.162	-0.0800
a_2	-0.091	-0.0981	-0.079	-0.1085

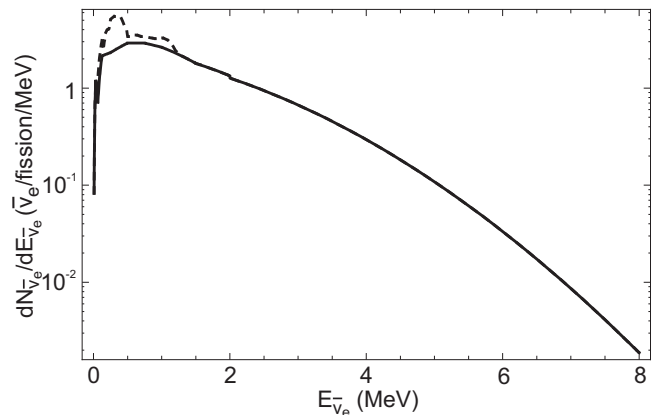
TABLE III. Low energy antineutrino spectra for each fissile isotope ($\bar{\nu}_e/\text{MeV}/\text{fission}$).

E [MeV]	^{235}U	^{239}Pu	^{238}U	^{241}Pu
2	1.26	1.08	1.5	1.32
1.5	1.69	1.48	1.97	1.75
1	2.41	2.32	2.75	2.63
0.75	2.66	2.58	2.96	2.9
0.5	2.66	2.63	2.91	2.82
0.25	2.16	2.08	2.18	2.14
0.125	1.98	1.99	2.02	1.85
6.25×10^{-2}	0.61	0.64	0.65	0.59
3.12×10^{-2}	0.35	2.13	1.32	3
1.563×10^{-2}	0.092	0.56	0.35	0.79
7.813×10^{-3}	0.024	0.14	0.089	0.2

can be translated to any experiment, by multiplying it by the number of fissions expected in the reactor, diminished by the distance factor.

V. CCD EXPERIMENT AT REACTOR

This work provides a preliminary analysis to forecast the expectations for the Coherent Neutrino-Nucleus Interaction Experiment (CONNIE), currently under construction. The goal of CONNIE is the first unambiguous

FIG. 7. Total reactor $N_{\bar{\nu}_e}$ spectrum per fission in the reactor per MeV. The solid line reflects the fissile isotopes, and the dashed line, the sum of the fissile isotopes and the neutron capture by ^{238}U .

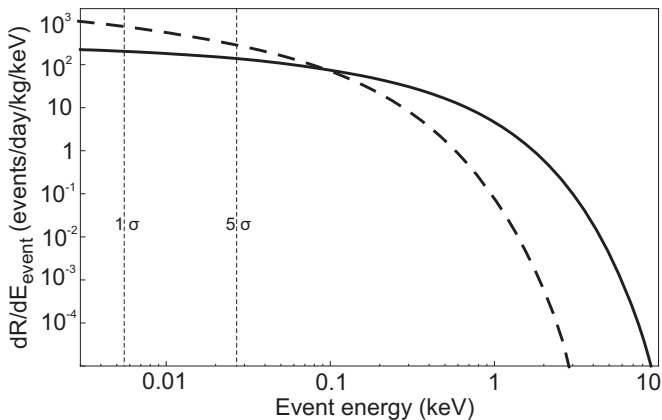


FIG. 8. Energy spectra for events expected in silicon detectors: the nuclear-recoil energy spectrum (—); the spectrum for detectable events (---), using the quenching factor from Lindhard, *et al.* [28, 29].

detection of neutrino-nucleus coherent scattering using an array of CCD detectors in a radiation shield located 30 meters from the core of the Angra II reactor, which operates at a thermal power of 3.95 GW. This experiment is planned to be installed at the Almirante Alvaro Alberto Nuclear Central, in Angra Dos Reis, Brazil during 2014.

In steady-state operation, the neutrino flux produced by the reactor is $1.21 \times 10^{20} \bar{\nu}_e/\text{s}$ approximately, and the flux density at the detector ($L = 30$ meters from the core) is $7.8 \times 10^{12} \bar{\nu}_e/\text{cm}^2/\text{s}$. These large numerical values justify the use of nuclear reactors as neutrino source for the CONNIE experiment.

The feasibility of neutrino detection close to a power nuclear reactor requires not only the estimation of the event rates and background noise, but also the proper identification of neutrino events. Once these parameters are known, the running time of the experiment to achieve a certain confidence level can be estimated.

A. Event rate

The product of the coherent scattering interaction is a nuclear recoil that ionizes electrons of Si atoms in the lattice, which are collected to form the event in the output image. Using the differential cross section, the total $\bar{\nu}_e$ spectrum and the $\bar{\nu}_e$ flux expected at the detector, the nuclear recoil spectrum $dR(E_{\text{rec}})/dE_{\text{rec}}$ is given by

$$\frac{dR}{dE_{\text{rec}}}(E_{\text{rec}}) = N_t \int_{\sqrt{\frac{2E_{\text{rec}}^2}{M}}}^{\infty} dE_{\bar{\nu}_e} \frac{dN_{\bar{\nu}_e}}{dE_{\bar{\nu}_e}}(E_{\bar{\nu}_e}) \times \frac{d\sigma}{dE_{\bar{\nu}_e} dE_{\text{rec}}}(E_{\bar{\nu}_e}, E_{\text{rec}}) \quad (4)$$

and the total rate for events R in the energy range of the detector is given by

$$R = \int_{E_{th}}^{\infty} dE_{\text{rec}} \frac{dR}{dE_{\text{rec}}}(E_{\text{rec}}) \quad (5)$$

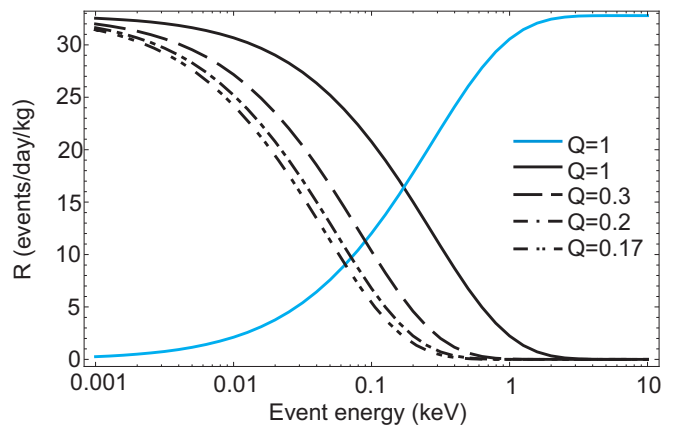


FIG. 9. Total number of events as a function of the threshold energy for different quenching factors: $Q = 1$, $Q = 0.3$, $Q = 0.2$ and $Q = 0.17$ (black curves). The light-blue curve shows the total number of events as a function of the maximum detectable recoil energy using $Q = 1$.

where $dN_{\bar{\nu}_e}(E_{\bar{\nu}_e})/dE_{\bar{\nu}_e}$ represents the spectrum of neutrinos at the detector, E_{th} is the detector's threshold energy, N_t is the number of nuclei in the detector, and $\sqrt{2E_{\text{rec}}^2/M}$ is the minimum neutrino energy that can produce a recoil with energy E_{rec} .

The results for dR/dE_{rec} and R from Eqs. (4) and (5) are shown in Fig. 8 and Fig. 9, respectively. The nuclear recoil spectrum shown in Fig. 8 decreases rapidly with energy. Although events with E_{rec} up to 10 keV are expected, any recoil for $E_{\text{rec}} > 3$ keV has a very low probability of occurrence. In fact, more than 96% of the events occur for $E_{\text{rec}} < 2$ keV. This behavior can be also deduced from the integrated spectrum in Fig. 9 (light-blue curve), which represents the rate of events as a function of the upper limit in E_{rec} . Above 2 keV, the distribution becomes flat and there is essentially no significant increase in the event rate. This characteristic should be used to find the best energy cutoff to maximize the event to background ratio. The bounded energy range also provides some clues about the expected signature from $\bar{\nu}_e$ -hits, as discussed in the next section. The use of heavier target materials result in an even shorter visible energy range.

Only a fraction of the nuclear recoil energy is converted into charge inside the Si detector, because part of the deposited energy results in phonons, contributing to the increase of the thermal energy of the system. The quantity that reflects the mean portion of the energy that is used in the ionizing process is the quenching factor Q . This factor has a strong dependence on energy and unfortunately it is not well known for energies < 4 keV, although there are several ongoing efforts to measure Q in this energy range [26]. However, measurements for event energies > 4 keV [27] agree with Lindhard's theory [28, 29]. Figure 10 shows the predicted silicon quenching factor by Lindhard, and the available measurements at different recoils energies. Taking into account the Lindhard

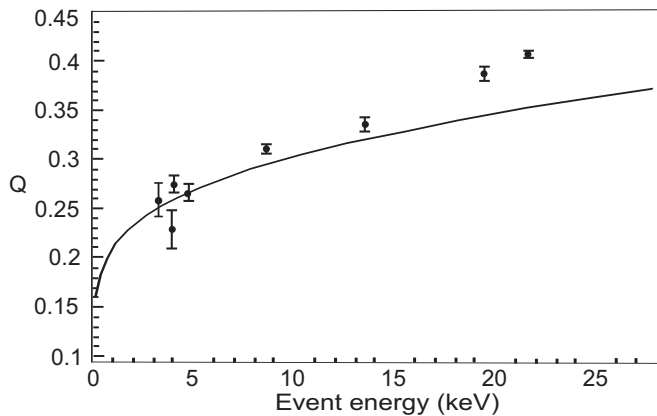


FIG. 10. Silicon quenching factor. Measurements from [27], and theoretical prediction from [28].

TABLE IV. Expected number of events for different quenching factors and threshold conditions, given in events/kg/day.

E_{th}	$Q = 1$	$Q = 0.3$	$Q = 0.2$	$Q = 0.17$
$1\sigma_{RMS}(5.5eV)$	30	29	28	27
$5\sigma_{RMS}(28eV)$	28	22	18	17

Q factor, the observable event energy spectrum is also shown as a dashed curve in Fig. 8, indicating that the range of ionization energy is reduced to approximately 3 keV. The dependence on lower ionizing energies becomes stronger due to the reduction of Q at small energy values.

Figure 9 also depicts the total number of detected events for different threshold energies and different values of the quenching factor Q (assuming Q is a constant). Despite the quenching factor is not well known at low energies, the total number of events detected has a relatively weak dependence on it because of the very low noise of CCD devices. Table IV summarizes the number of events per day per kg of detector for different quenching factors and for two values of energy threshold E_{th} . The total number of events for zero energy threshold is expected to be 33 events per day per kg of silicon.

B. Identification of neutrino candidate events

The low energy nuclear recoil signature in the CCD corresponds to a diffusion limited hit, which means that the observed charge is generated in a volume smaller than the pixel size, and the event is formed only by the diffusion of the free charge in the silicon [10].

When the charge is free to move in the Si lattice, the diffusion and drift mechanisms define its final lateral dispersion before it is trapped by the electric potential well under the gates. As it was explained in section II, the lateral barriers extend approximately 10 μm in depth (y axes). Beyond this point, the electric field in the entire silicon bulk is uniform along the x and z axis, and varies

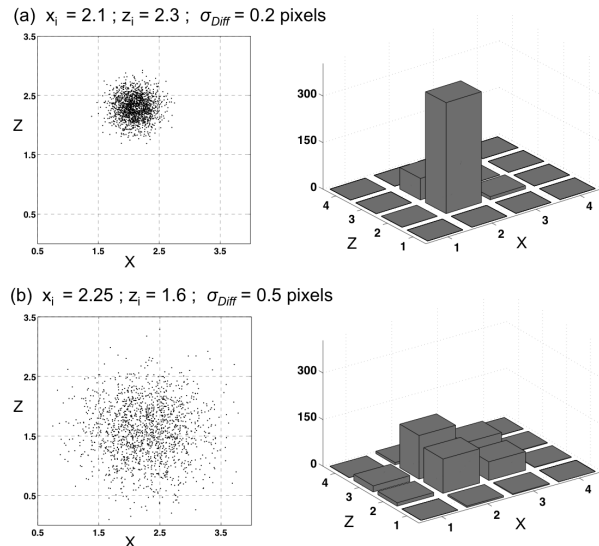


FIG. 11. Two simulated neutrino events generated at different depths of the detector and at different relative position in the pixel. (a) $\bar{\nu}_e$ -event interacting close to the gates of the detector, with $\sigma_{Diff} = 0.2$ pixels, and (b) $\bar{\nu}_e$ -event interacting close to the back (large y) of the detector, where $\sigma_{Diff} = 0.5$ pixels. The x_i and z_i values are the coordinates of the point of origin of the events in the array.

only as a linear function of y (a detailed electrostatic description of the devices can be found in [17]). The net result is that most of the carriers reach the well of the gate in the same pixel in which they were generated, and only a small fraction transverse to adjacent pixels.

The ‘‘pixelation’’ of the detector plays an important role in the final shape of the expected event, giving a 2D stepped representation of the Gaussian distribution expected from diffusion. Due to the small number of pixels that form the event, the shape of the stepped distribution depends strongly on the initial lateral position of the charge relative to the boundaries of the pixel. Figure 11 shows the effect of diffusion and pixelation on a simulated neutrino event produced at different depths and lateral positions. The energy of the event is 1.6 keV and it is simulated as interacting very close to the gates of the CCD in the y axes (standard deviation of the diffusion distribution: $\sigma_{Diff} = 0.2$ pixels) with a lateral position of $(x_i, z_i) = (2.1, 2.3)$ pixels in the array, in Fig. 11(a), and at $y \approx 250 \mu\text{m}$ at the back of the detector ($\sigma_{Diff} = 0.5$ pixels) with $(x_i, z_i) = (2.25, 1.6)$ in Fig. 11(b). A detailed description of the shape of diffusion limited hits can be found in [10, 19, 26, 30].

The energy calibration of CCDs can be performed using several standard procedures. The most intuitive technique is using an X-ray source, specially ^{55}Fe . A full description of the procedure can be found in [9], and the calibration for these detectors in [10, 26].

TABLE V. Expected number of events in the CCD array, for a mass of 52 g, for different quenching factors and threshold conditions. Results are given in units of events/day (events/year).

E_{th}	$Q = 1$	$Q = 0.3$	$Q = 0.2$	$Q = 0.17$
$1\sigma_{RMS}$ (5.5eV)	1.56 (569)	1.5 (547)	1.46 (532)	1.4 (511)
$5\sigma_{RMS}$ (28eV)	1.46 (533)	1.14 (416)	0.94 (343)	0.9 (328)

C. Running conditions and forecast

The current version of the CONNIE detector is based on 10 CCD running in parallel. The CCD setup has capacity to read CCD of any thickness, and array sizes of up to approximately 6 cm by 6 cm. The system was designed for easy on-site replacement of detectors. After a preliminary operating stage, ten 5.2 g CCD units are planned to be running, summing 52 grams of detecting mass. The final spectrum and rate of events can be calculated from Figs. 8 and 9, respectively. The number of expected events is 1.716 per day, totaling 626 events per year. Different conditions for anticipated Q and threshold energies are summarized in Table V.

To provide a first-order calculation of the expected running time, the result can be viewed as a counting experiment for a signal, expected to be higher than the Poisson fluctuation of the background at some given confidence level, for any specified range of energy.

Available bibliography shows that the count rate from background events in the low energy region at sea level using passive shield can be reduced to ≈ 600 events/KeV/day/Kg [31], assuming that the material of the shield has a low level of radiative contamination. Similar rates of background have been reached using similar configurations of CCD at shallow depth (30 m.w.e) in the Minos tunnel at Fermilab, and deep underground (600 m.w.e) at Snolab [10, 26].

Figure 9 shows that for $Q < 0.3$ almost all event have an ionization energy of < 300 eV. The energy range of our interest lies between 28 eV ($5\sigma_{RMS}$) and 300 eV. Assuming $Q = 0.2$, the event rate from Table V yields 0.94 events/day for a 52 g array of CCD.

The background noise can also be scaled by the mass of the detector and by the energy interval resulting in a rate of 8.5 events/day. A signal-to-noise ratio defined as $0.94T/2.91\sqrt{T} = 0.32\sqrt{T}$ where T is the running time in days, can be used to obtain the corresponding confidence value. Therefore, the number of days running the experiment to achieve a certain confidence level (CL) can be computed, and some values for several CL values are listed in Table VI.

TABLE VI. Expected running time for achieving different CL [PDG].

CL [%]	T [days]
80.00	07
90.00	16
95.00	27
98.00	44
99.87	87

VI. CONCLUSION

The capabilities of Charge Coupled Devices to detect coherent neutrino-nucleus scattering interaction has been demonstrated. The small threshold achieved on these devices allows the detection of small depositions of energy, in particular, nuclear recoils from neutrino scattering. On this energy range, the interaction occurrence is enhanced by coherence and therefore the neutrino signal can be observed using a system with moderate detecting mass.

The basis for a coherent neutrino nucleus scattering experiment at a nuclear reactor have been also reviewed. The article shows that a neutrino signal of 626 events per year can expected in a CCD array of 52 g, with a certainty greater than 99% over the background fluctuation after ninety days of measurements.

VII. ACKNOWLEDGMENTS

The authors wish to thank Dr. Tom Ferbel, University of Rochester, for his review of an early draft, and his many suggestions.

-
- [1] F. J. Hasert et al., Phys. Lett B **46**, 121 (1973).
 - [2] D. Z. Freedman, Phys. Rev. D **9**, 1389 (1974).
 - [3] D. Z. Freedman, D. N. Schramm and D. L. Tubbs, Annu. Rev. Nucl. Part. Sci., **27**, 167 (1977).
 - [4] K. Scholberg, Phys. Rev. D **73**, 033005 (2006).
 - [5] P. S. Barbeau, J. I. Collar, J. Miyamoto and I. Shipsey, IEEE Trans. Nucl. Sci. **50**, 1285 (2003).
 - [6] C. Hagmann and A. Bemstein, IEEE Trans. Nucl. Sci **51**, 2151 (2004).
 - [7] W.S. Boyle, Rev. Mod. Phys. **82**, 2305 (2010).
 - [8] G.E. Smith, Rev. Mod. Phys. **82**, 2307 (2010).
 - [9] J.R. Janesick, *Scientific Charge Coupled Devices*, (SPIE Publications, Bellingham, Washington, 2001).
 - [10] J. Barreto et al, Physics Letters B **711**, 264 (2012).
 - [11] K. A. Hochmuth, M. Lindner and G. G. Raffelt, Phys. Rev. D **76**, 073001 (2007).
 - [12] F. Boehm, Results from the Palo Verde neutrino oscillation experiment, Phys. Rev. D **62**, 072002 (2000).
 - [13] K. Nakajima, K Inoue, K. Owada, F. Suekane, A. Suzuki, G. Hirano, S. Kosaka and T. Ohta, H. Tanaka, Nucl.

- Instrum. Methods **A569**, 837 (2006).
- [14] B. Xin, Phys. Rev. D **72**, 012006 (2005).
- [15] H. T. Wong, Phys. Rev. D **75**, 012001 (2007).
- [16] H. Oluseyo, R. Meynart, S.P. Neeck and H. Shimoda, Proc. of SPIE **5570**, 515 (2004).
- [17] S.E.Holland, D. E. Groom, N. P. Palaio, F. J. Stover and M. W., IEEE Trans. Electron Devices **50**, 225 (2003).
- [18] Estrada, J. et al., Proc. of SPIE **6269**, 62693 (2006).
- [19] J. Estrada, J. Molina, J. J. Blostein, G. Fernandez Moroni, Nucl. Instrum. Methods in Phys. Res. Sect. **665**, 90 (2011).
- [20] G. I. Cancelo, J. C. Estrada, G. Fernandez Moroni, K. Treptow, T. Zmuda, H. T. Diehl, Experimental Astronomy **34**, 13 (2012).
- [21] G. Fernandez Moroni, J. Estrada, G. Cancelo, S. E. Holland, E. E. Paolini, H. T. Diehl, Experimental Astronomy **34**, 43 (2012).
- [22] K. Zuber, *Neutrino Physics* (CRC Press, Boca Raton, FL., 2011).
- [23] K. Patton, et al, Phys. Rev. C **86**, 024612 (2012).
- [24] P. Vogel, G. K. Schenter, F. M. Mann and R. E. Schenter, Phys. Rev. C **24**, 1543 (1981).
- [25] P. Vogel and J. Engel, Phys. Rev. D **39**, 3378 (1989).
- [26] J. S. Tiffenberg *et al.*, in *Proceedings of the 33rd International Cosmic Ray Conference (ICRC2013)*, Rio de Janeiro, 2013.
- [27] J.D. Lewin and P.F. Smith, Astropart. Phys. **6**, 87 (1996).
- [28] J. Lindhard, V. Nielsen, M. Scharff and P.V. Thomsen, Mat. Fys. Medd. Dan. Selsk. **33**, 10 (1963).
- [29] H. Chagani *et al.*, J. Inst. **3**, 06003 (2008).
- [30] G. Fernandez Moroni, E. E. Paolini, J. Estrada, G. I. Cancelo, in *Proceeding of the Reunion de Trabajo en Procesamiento de la Informacion y Control (2013)*, Bariloche, 2013.
- [31] G. Heusser, Annu. Rev. Nucl. and Part. Sci. **45**, 543 (1995).